

MTE1 Functions with MPH1 in Double-Strand Break Repair

Askar Yimit,^{*,†} TaeHyung Kim,^{†,‡} Ranjith P. Anand,[§] Sarah Meister,^{*,†} Jiongwen Ou,^{*,†} James E. Haber,[§]
Zhaolei Zhang,^{†,‡} and Grant W. Brown^{*,†,1}

^{*}Department of Biochemistry, [†]Donnelly Centre, and [‡]Department of Computer Science, University of Toronto, Toronto, Ontario M5S 3E1, Canada, and [§]Rosenstiel Basic Medical Sciences Research Center, Brandeis University, Waltham, Massachusetts 02453

ORCID ID: 0000-0002-9002-5003 (G.W.B.)

ABSTRACT Double-strand DNA breaks occur upon exposure of cells to ionizing radiation and certain chemical agents or indirectly through replication fork collapse at DNA damage sites. If left unrepaired, double-strand breaks can cause genome instability and cell death, and their repair can result in loss of heterozygosity. In response to DNA damage, proteins involved in double-strand break repair by homologous recombination relocalize into discrete nuclear foci. We identified 29 proteins that colocalize with recombination repair protein Rad52 in response to DNA damage. Of particular interest, Ygr042w/Mte1, a protein of unknown function, showed robust colocalization with Rad52. Mte1 foci fail to form when the DNA helicase gene *MPH1* is absent. Mte1 and Mph1 form a complex and are recruited to double-strand breaks *in vivo* in a mutually dependent manner. *MTE1* is important for resolution of Rad52 foci during double-strand break repair and for suppressing break-induced replication. Together our data indicate that Mte1 functions with Mph1 in double-strand break repair.

KEYWORDS DNA repair; recombination; double-strand breaks; break-induced replication; loss of heterozygosity; nuclear foci

EFFECTIVE repair of double-strand DNA breaks (DSBs) is critical to the preservation of genome stability, yet most modes of DSB repair have significant potential to generate sequence alterations or sequence loss. Repair of DSBs by homologous recombination can result in loss of heterozygosity when resolution of recombination intermediates between homologous chromosomes results in a crossover. As such, cells possess several mechanisms by which crossing over can be suppressed in favor of noncrossover recombination products. Double Holliday junction (dHJ) intermediates that result from invasion of a homologous chromosome by both ends of a resected DSB (Szostak *et al.* 1983) can be resolved nucleolytically by the action of the Yen1 and Mus81/Mms4 endonucleases (Blanco *et al.* 2010; Ho *et al.* 2010) to produce a random distribution of crossover and noncrossover products. By contrast, the same dHJ intermediates can be dissolved by the

combined helicase and ssDNA decatenase action of the Bloom/TopIII α /Rmi1 complex (Sgs1/Top3/Rmi1 in yeast) (Wu *et al.* 2006; Yang *et al.* 2010) to yield exclusively noncrossover products (Wu and Hickson 2003). Crossovers can also be prevented if the D-loop structure that results from the first strand invasion by one end of a resected DSB into the homologous chromosome is unwound before capture of the second end to form the dHJ. Unwinding of D-loops is catalyzed *in vitro* and *in vivo* by the 3'-to-5' DNA helicase Mph1 (Sun *et al.* 2008; Prakash *et al.* 2009) to prevent loss of heterozygosity due to crossovers and break-induced replication (BIR) (Luke-Glaser and Luke 2012; Mazon and Symington 2013; Stafa *et al.* 2014).

The Mph1 DNA helicase was first identified as a deletion mutant with an increased mutation frequency (Entian *et al.* 1999). Subsequent characterization revealed that *mph1* mutants are sensitive to the alkylating agent MMS and to a lesser degree to ionizing radiation (Scheller *et al.* 2000), and that *mph1* mutants are proficient for mitotic recombination (Schurer *et al.* 2004). Molecular insight into Mph1 function in recombination reactions comes from evidence that Mph1 is a DNA helicase (Prakash *et al.* 2005), and that Mph1 can unwind Rad51 D-loops (Sun *et al.* 2008; Prakash *et al.* 2009) and extended D-loops (Sebesta *et al.* 2011). Consistent with an antirecombination role for Mph1, overexpression of

Copyright © 2016 by the Genetics Society of America
doi: 10.1534/genetics.115.185454

Manuscript received November 29, 2015; accepted for publication February 22, 2016;
published Early Online February 24, 2016.

Supplemental material is available online at www.genetics.org/lookup/suppl/doi:10.1534/genetics.115.185454/-/DC1.

¹Corresponding author: Department of Biochemistry, University of Toronto, Donnelly Centre, Room 1206, 160 College St., Toronto, Ontario M5S 3E1, Canada.
E-mail: grant.brown@utoronto.ca

MPH1 reduces recombination rate and reduces loading of Rad51 at an induced DSB (Banerjee *et al.* 2008). Indeed, Mph1 suppresses crossing over during mitotic recombination, likely by unwinding D-loop recombination intermediates formed by Rad51 (Prakash *et al.* 2009) and preventing ectopic resolution of early strand exchange intermediates by the Mus81–Mms4 nuclease (Mazon and Symington 2013). Mph1 inhibits BIR repair of double-strand breaks (Luke-Glaser and Luke 2012) and promotes template switching during BIR (Stafa *et al.* 2014), both consistent with the ability of Mph1 to unwind recombination intermediates *in vitro*. In addition to functioning in crossover suppression, Mph1 plays a prorecombinogenic role in repair of stressed DNA replication forks (Sun *et al.* 2008; Chen *et al.* 2009, 2013; Choi *et al.* 2010; Chavez *et al.* 2011; Zheng *et al.* 2011; Xue *et al.* 2014) and inhibits nonhomologous end-joining repair at telomeres (Luke-Glaser and Luke 2012). Mph1 is thought to be the functional homolog of the human FANCM protein (Kee and D’Andrea 2010; Whitby 2010; Xue *et al.* 2015). Thus, available evidence points to diverse functions for Mph1, and these functions are likely connected to the ability of Mph1 to unwind and remodel DNA structures.

Here we leverage intracellular protein location data to identify the complement of proteins that colocalize with the recombination repair protein Rad52 in nuclear foci during the response to DNA double-strand breaks. In addition to defining the membership of Rad52 foci, we identify an uncharacterized protein, Ygr042w/Mte1, that functions in double-strand break repair. Mte1 acts in complex with Mph1 at double-strand breaks *in vivo*, is important for DSB repair as assessed by resolution of Rad52 foci, and functions, as is the case for Mph1, in suppressing BIR repair of double-strand DNA breaks.

Materials and Methods

Yeast strains and media

All yeast strains used in this study are derivatives of BY4741 (Brachmann *et al.* 1998), CL11-7, or W303, and are listed in Supplemental Material, Table S1. Strains were constructed using genetic crosses and standard PCR-based gene disruption techniques. Standard yeast media and growth conditions were used.

Chromatin immunoprecipitation and deep sequencing

Chromatin immunoprecipitation (IP) was performed using Flag-epitope-tagged versions of each indicated protein, as previously described (Roberts *et al.* 2008; Balint *et al.* 2015), with modifications. Cells were grown to midlogarithmic phase in YPR (1% yeast extract, 2% peptone, 3% raffinose) at 28° and then arrested in G2/M with 20 µg/ml nocodazole for 4 hr. Galactose was added to 2% final concentration to induce expression of the *HO* endonuclease gene. Cells were sampled before galactose addition and after 4 hr of induction and cross-linked with formaldehyde overnight. Cells were harvested and washed twice with cold TBS (20 mM Tris-HCl pH

7.5, 150 mM NaCl), resuspended in FA-lysis buffer (50 mM HEPES pH 7.5, 2 mM EDTA, 1% Triton X-100, 0.1% sodium deoxycholate, 150 mM NaCl) containing 0.05% SDS, lysed, and sonicated. Immunoprecipitates were washed sequentially with 1 ml of FA-lysis buffer, FA-lysis buffer containing 1 M NaCl, FA-lysis buffer containing 0.5 M NaCl, wash buffer (50 mM HEPES pH 7.5, 0.25 M LiCl, 2 mM EDTA, 1% Triton X-100, 1% sodium deoxycholate, 1% NP-40, 10 mM Tris-HCl pH 8.0), and TE (10 mM Tris-HCl pH 8.0, 1 mM EDTA). Protein–DNA complexes were eluted, cross-links were reversed, protein and RNA was digested, and DNA was isolated by phenol/chloroform extraction and ethanol precipitation. Sequencing libraries were generated using the Nextera XT DNA Sample Preparation Kit (Illumina) with custom index primers for the PCR amplification step. Libraries were quantified using a 2100 Bioanalyzer (Agilent) and the KAPA SYBR FAST Universal qPCR Kit (KAPA Biosystems).

Sequencing data analysis

Input and IP samples from each experiment were sequenced on an Illumina HiSeq 2500 (50 nucleotide single-end reads). All sequencing data are deposited in the Sequence Read Archive (<http://www.ncbi.nlm.nih.gov/sra>, study accession SRP064493). The number of reads for each sample ranges from 12.8 M to 25.7 M. The quality of sequencing reads was first assessed using FastQC (<http://www.bioinformatics.bbsrc.ac.uk/projects/fastqc>). All samples have a median PHRED score of ≥ 30 for all positions. Sequenced reads were mapped to the *Saccharomyces cerevisiae* reference genome version WS220 (downloaded from the *Saccharomyces* Genome Database) (Cherry *et al.* 2012; Engel *et al.* 2014) using Bowtie2 (version 2.0.0) (Langmead and Salzberg 2012) with default settings, except for forcing end-to-end alignment. Greater than 96% mapping frequencies were achieved for all samples, yielding a minimum 50× coverage for all samples (Table S2). To reduce any bias from DNA sequencing, the data were normalized by the ratio of coverage for each IP and input pair prior to each comparison. We used a 100-bp sliding window with a step size of 50 bp to calculate enrichment scores as a \log_2 ratio of normalized read counts for each IP:input pair. The enrichment scores for all of IP:input pairs, plotted across chromosome III, are shown in Figure 5.

Whole cell extracts, immunoblotting, and immunoprecipitation

Logarithmically growing cells at 30° were treated with or without 5 µg/ml phleomycin (BioShop PEO422.25) for 2 hr before cells were collected, fixed with 10% trichloroacetic acid, and whole cell extracts were prepared (Pelliccioli *et al.* 1999). Proteins were resolved by SDS-PAGE and subjected to immunoblotting with α -Flag M2 (F3165, Sigma-Aldrich), α -HA (ab16918, Abcam), or α -tubulin (YOL1/34, Serotec) antibodies. Native extracts for immunoprecipitation were prepared from 5×10^8 cells as previously described (Shimomura *et al.* 1998), with some modifications. Cell pellets were resuspended in FA-lysis buffer containing 1 mM DTT,

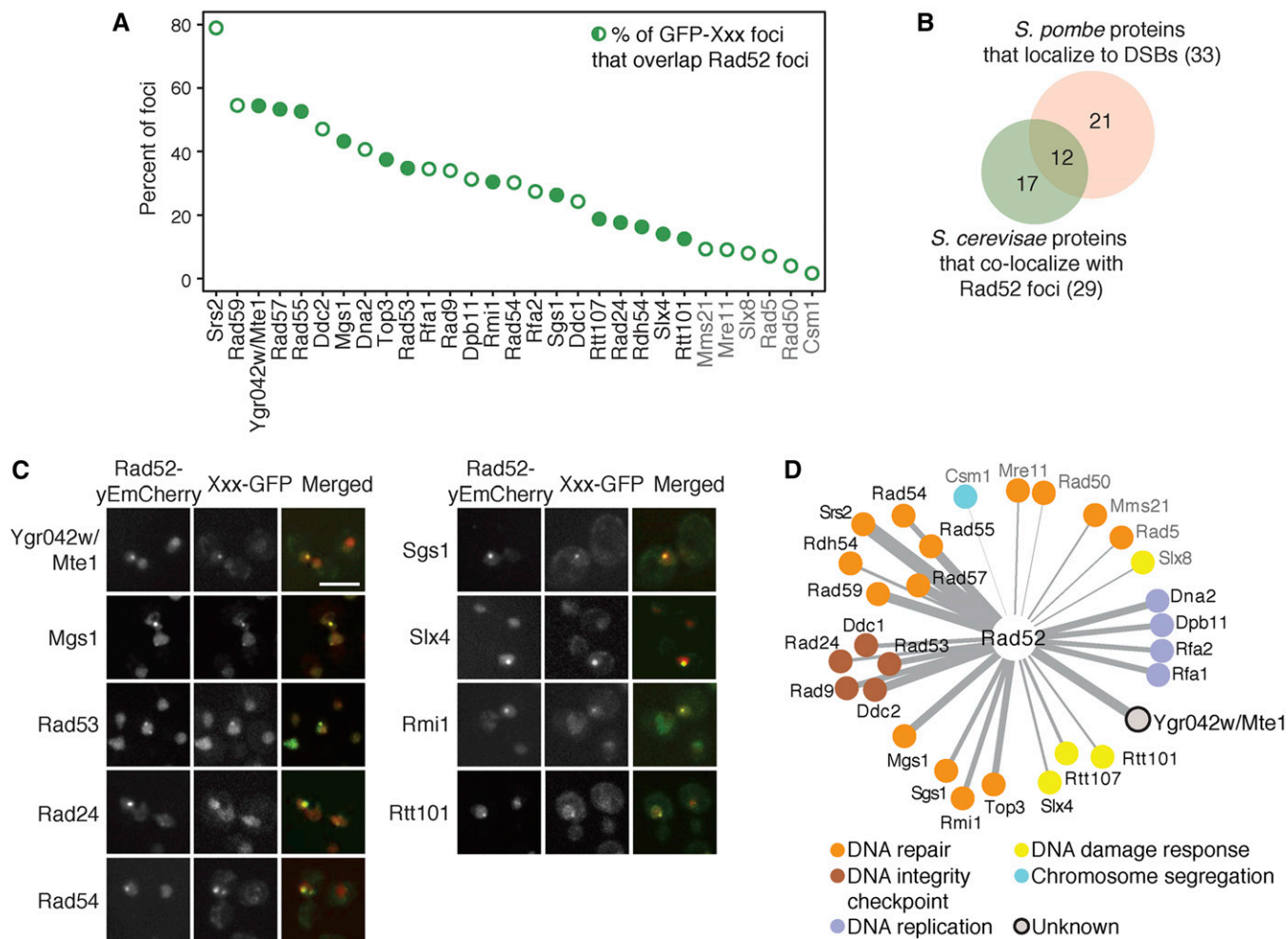


Figure 1 Twenty-nine proteins form nuclear foci that detectably colocalize with Rad52 foci. (A) The percent of nuclear foci formed by each GFP fusion protein that overlaps with Rad52-yEmCherry foci after 2 hr in 5 μ g/ml phleomycin is plotted. Open circles indicate colocalizations that were previously identified. Closed circles indicate Rad52 colocalizations that have not been previously described. Protein names in gray indicate those with a percent colocalization at or below that seen with Mre11. (B) The overlap between the proteins that colocalize with Rad52 foci and those that colocalize with an induced double-strand DNA break in fission yeast is shown. (C) Representative fluorescence micrographs showing colocalization of the indicated GFP fusion proteins with Rad52 foci. The mCherry, GFP, and merged images are shown. Bar, 5 μ m. (D) A network of the proteins that colocalize detectably with Rad52. Protein function is indicated by color and edge thickness is proportional to the extent of protein colocalization with Rad52 foci.

2 mM sodium fluoride, 1 mM sodium orthovanadate, 1 \times Complete Mini EDTA-free protease inhibitor cocktail (Roche 11836170001), 2.5 μ g/ml aprotinin, 10 mM β -glycerophosphate, 5 μ g/ml leupeptin, 2 μ g/ml pepstatin A, 1 mM PMSF, and 5 μ g/ml tosyl-L-lysyl-chloromethane hydrochloride, and then lysed with glass beads. Cleared extracts were immunoprecipitated with α -Flag M2 antibody. Beads were washed twice with 0.5 ml FA-lysis buffer as above and eluted in 5 \times SDS loading buffer.

DNA damage sensitivity

Yeast strains were grown overnight in YPD, diluted serially, and spotted onto YPD plates containing the indicated concentrations of phleomycin. Plates were incubated at 30 $^\circ$ for 2–3 days before imaging. The experiment was repeated twice, and a representative example is shown.

Fluorescence microscopy

For analysis of GFP fusion protein nuclear foci, strains were grown to midlog phase in YPD, diluted into fresh YPD and cultured overnight to OD₆₀₀ = 0.3. Cells were treated for 120 min with 5 μ g/ml phleomycin, or cultured without phleomycin, harvested, and washed once in low fluorescence medium with or without phleomycin before imaging. Eleven z slices with a 0.4- μ m step size were acquired using Volocity imaging software (PerkinElmer) controlling a Leica DMI6000 confocal fluorescence microscope with fluorescein isothiocyanate, Texas Red, and differential interference contrast filter sets (Quorum Technologies). Images were scored by visual inspection for GFP fusion protein foci. Samples were compared using the t -test or the Wilcoxon rank sum test, as appropriate, in R

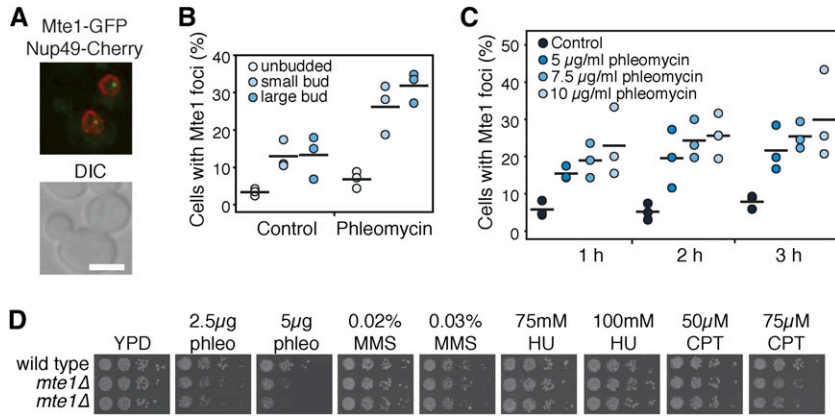


Figure 2 Mte1 foci form in S/G2 phase and in response to double-strand breaks. (A) Mte1–GFP nuclear foci are shown in a merged fluorescence micrograph. The lower panel is the DIC image of the same cells. Bar, 5 μ m. (B) The percent of cells in each morphology category (unbudded, small-budded, and large-budded) with Mte1 nuclear foci after 2 hr in 5 μ g/ml phleomycin, or untreated, is plotted. The solid bars show the means of the three replicates. *N* ranged from 46 to 188 cells per morphology category per replicate. (C) The percent of cells with Mte1 nuclear foci after 1, 2, or 3 hr in the indicated concentrations of phleomycin is plotted. The solid bars show the means of the three replicates. *N* ranged from 60 to 166 cells per drug concentration per replicate. (D) Serial 10-fold dilutions of the indicated strains were spotted on the indicated concentrations of phleomycin (phleo), methyl methanesulfonate (MMS), hydroxyurea (HU), or camptothecin (CPT). Plates were photographed after 2–3 days.

(www.r-project.org). Data were plotted using ggplot2 in R. For Rad52–GFP foci, the same procedure was used except that cells were blocked in G2/M phase by treatment with 20 μ g/ml nocodazole for 3 hr and exposed to 50 μ g/ml

phleomycin for 30 min. To screen Mte1–GFP foci in different mutant backgrounds, we imaged a single *z*-slice on an EVOTEC Opera confocal microscope system (PerkinElmer), as described (Tkach *et al.* 2012).

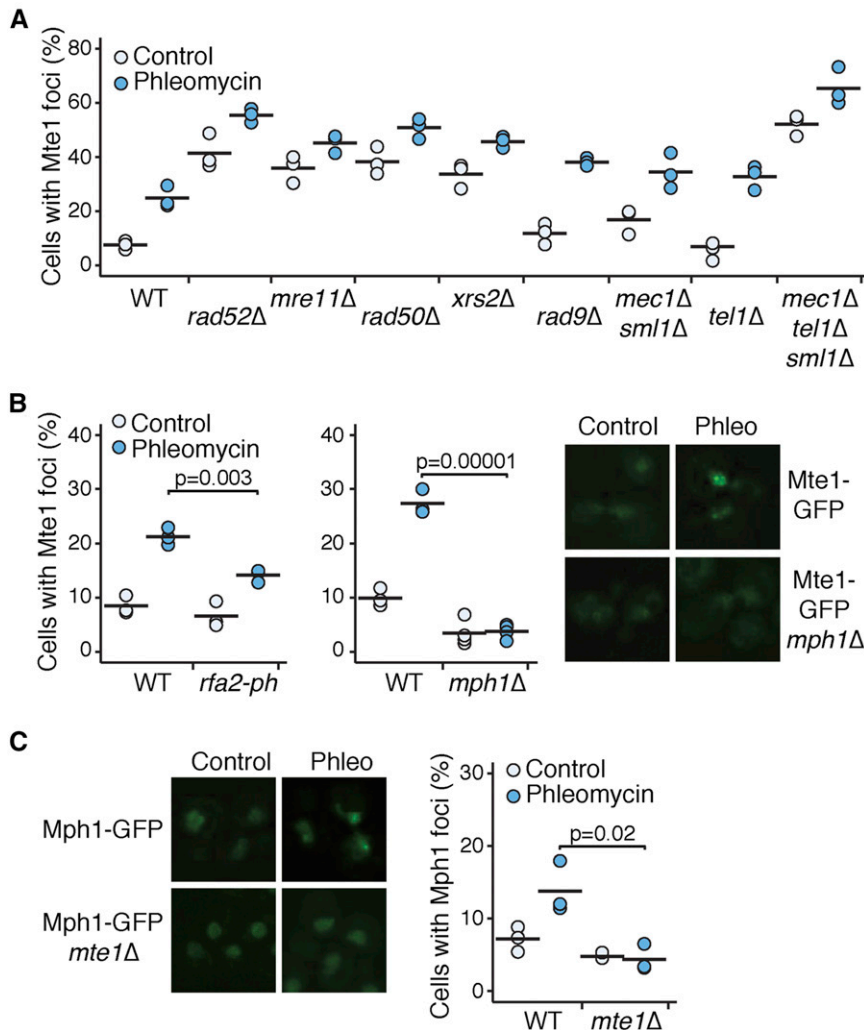


Figure 3 Mte1 foci are increased in *MRX* mutants and depend on *MPH1*. (A) The percent of cells with Mte1 foci is plotted for mutants with increased numbers of foci. Three replicates for each strain, in the absence and presence of 5 μ g/ml phleomycin, are plotted. The black bars show the means of the three replicates. *N* ranged from 41 to 211 cells per strain per replicate. (B) The percent of cells with Mte1 foci is plotted for mutants with decreased numbers of foci (left) for untreated cells and cells grown in the presence of 5 μ g/ml phleomycin for 2 hr. The black bars show the means of the replicates. The indicated samples were compared using a one-sided *t*-test. *N* ranged from 65 to 174 cells per strain per replicate. Representative images (right) of cells with Mte1 foci are shown for untreated cells and cells grown in the presence of 5 μ g/ml phleomycin for 2 hr, for wild-type cells, and *mph1Δ* cells. (C) Representative images (left) and the percent of cells with Mph1 foci (right) are shown for untreated cells and cells grown in the presence of 5 μ g/ml phleomycin for 2 hr, for wild-type cells and *mte1Δ* cells. The black bars show the means of the replicates. The indicated samples were compared using a one-sided *t*-test. *N* ranged from 89 to 276 cells per strain per replicate.

Recombination assays

Recombination rates (events/cell/generation) were calculated using a direct repeat recombination assay (Smith and Rothstein 1999) and quantifying recombination from the number of Leu⁺ recombinant colonies using the method of the median (Lea and Coulson 1949). Each fluctuation test comprised nine independent cultures, and the results from 10 fluctuation tests were plotted in R. Rates were compared using a Welch two-sample *t*-test in R.

BIR efficiencies were calculated as described previously (Anand *et al.* 2014). Briefly, cells were plated for individual colonies on YEPD + clonNat to retain the HOcs (which is marked with *natMX*). Approximately 1 million cells from individual colonies were appropriately diluted and plated on YEPD plates to get the total cell count and on YEP-Gal plates for *HO* induction. Cells that grew on YEP-Gal plates (DNA break survivors) were counted and replica plated to plates lacking uracil to determine BIR frequencies. For each replicate, Ura⁺ frequencies were calculated as total Ura⁺ cells that grew on plates lacking uracil over total cells that grew on YEPD. Experiments were repeated at least three times, plotted in R, and compared using a Welch two-sample *t*-test in R.

Data availability

Strains are available upon request. Table S1 contains the genotypes of all strains used. Table S2 contains statistics for all deep sequencing, including NCBI Sequence Read Archive (SRA) accession numbers.

Results

Twenty-nine proteins form nuclear foci that detectably colocalize with Rad52 foci

A number of DNA repair proteins change their intracellular localization from pannuclear to nuclear foci in response to DNA damage. Proteins that localize in nuclear foci have been identified in candidate approaches (Lisby *et al.* 2001, 2004; Melo *et al.* 2001; Zhu *et al.* 2008; Burgess *et al.* 2009; Germann *et al.* 2011) and in genome-scale screens (Tkach *et al.* 2012; Denervaud *et al.* 2013; Mazumder *et al.* 2013; Yu *et al.* 2013). Nuclear foci are commonly thought of as centers of DNA repair, in part because foci formed by recombination repair proteins colocalize with double-strand DNA breaks (Lisby *et al.* 2003). However, not all nuclear foci are identical to the canonical DNA repair centers that are marked by the recombination protein Rad52. For example, Cmr1 forms foci that do not colocalize detectably with Rad52 (Tkach *et al.* 2012), but rather colocalize with a distinct set of proteins in an intranuclear quality control compartment (Gallina *et al.* 2015).

We tested 61 budding yeast proteins that form nuclear foci in response to DNA damage to identify those that colocalize detectably with Rad52. Nuclear foci proteins were tagged with GFP (Huh *et al.* 2003), Rad52 was tagged with mCherry, and cells were examined by fluorescence

microscopy after treatment with the double-strand DNA break-inducing agent phleomycin (Figure 1). Twenty-nine proteins colocalized detectably with Rad52 (Figure 1A, Table S3, Table S4, and Table S5). The extent of colocalization ranged from 79% of foci for Srs2 to 2% of foci for Csm1 (Table S3). Six colocalizations we regard with caution, as the extent of colocalization was equal or less than that seen with Mre11 (indicated in gray in Figure 1). A low extent of Mre11 colocalization with Rad52 has been observed previously and attributed to colocalization of DSBs that are at different stages of repair (Lisby *et al.* 2004). Fourteen proteins had not previously been described as components of Rad52 foci (Figure 1, A and C), although most are known DNA repair, DNA replication, or checkpoint signaling proteins (Figure 1D). We identified one protein, Ygr042w, with no known role in recombination repair. Mutants in *YGR042W* affect telomere length (Askree *et al.* 2004), and the fission yeast homolog of Ygr042w, Dbl2, forms foci that colocalize with an induced double-strand DNA break (Yu *et al.* 2013). The extensive colocalization of Ygr042w with Rad52 foci, similar to the extent of colocalization observed for members of the Rad52 epistasis group (Symington 2002) Rad55, Rad57, and Rad59, suggests that Ygr042w could function in repair of double-strand DNA breaks. While this work was in progress, a name for *YGR042W* was reserved in the *Saccharomyces* Genome Database, *MTE1* (Mph1-associated

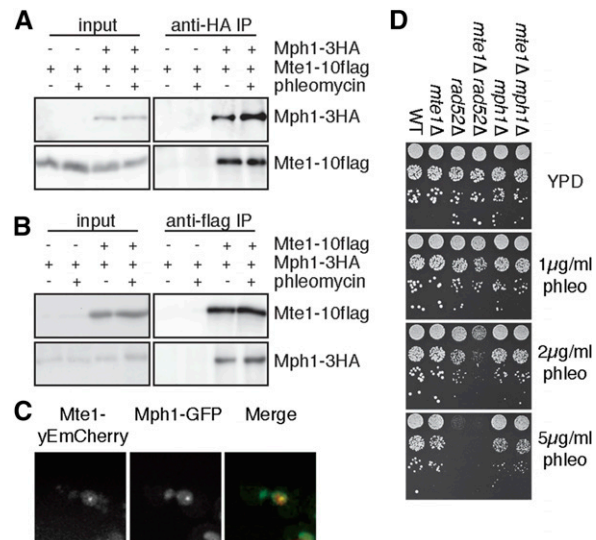


Figure 4 Mte1 and Mph1 interact physically and are in the same genetic pathway. (A) Extracts of cells expressing Mte1–10flag and Mph1–3HA proteins as indicated were subjected to immunoprecipitation with an anti-HA antibody. Input and immunoprecipitate (IP) fractions were immunoblotted to detect Mte1–10flag or Mph1–3HA. (B) In the reciprocal of A, extracts of cells expressing Mte1–10flag and Mph1–3HA proteins as indicated were subjected to immunoprecipitation with an anti-flag antibody. Input and IP fractions were immunoblotted to detect Mte1–10flag or Mph1–3HA. (C) Representative fluorescence micrographs showing colocalization of Mte1 with Mph1 following phleomycin treatment. The mCherry, GFP, and merged images are shown. (D) Serial 10-fold dilutions of the indicated strains were spotted on media containing the indicated concentrations of phleomycin. Plates were photographed after 2–3 days.

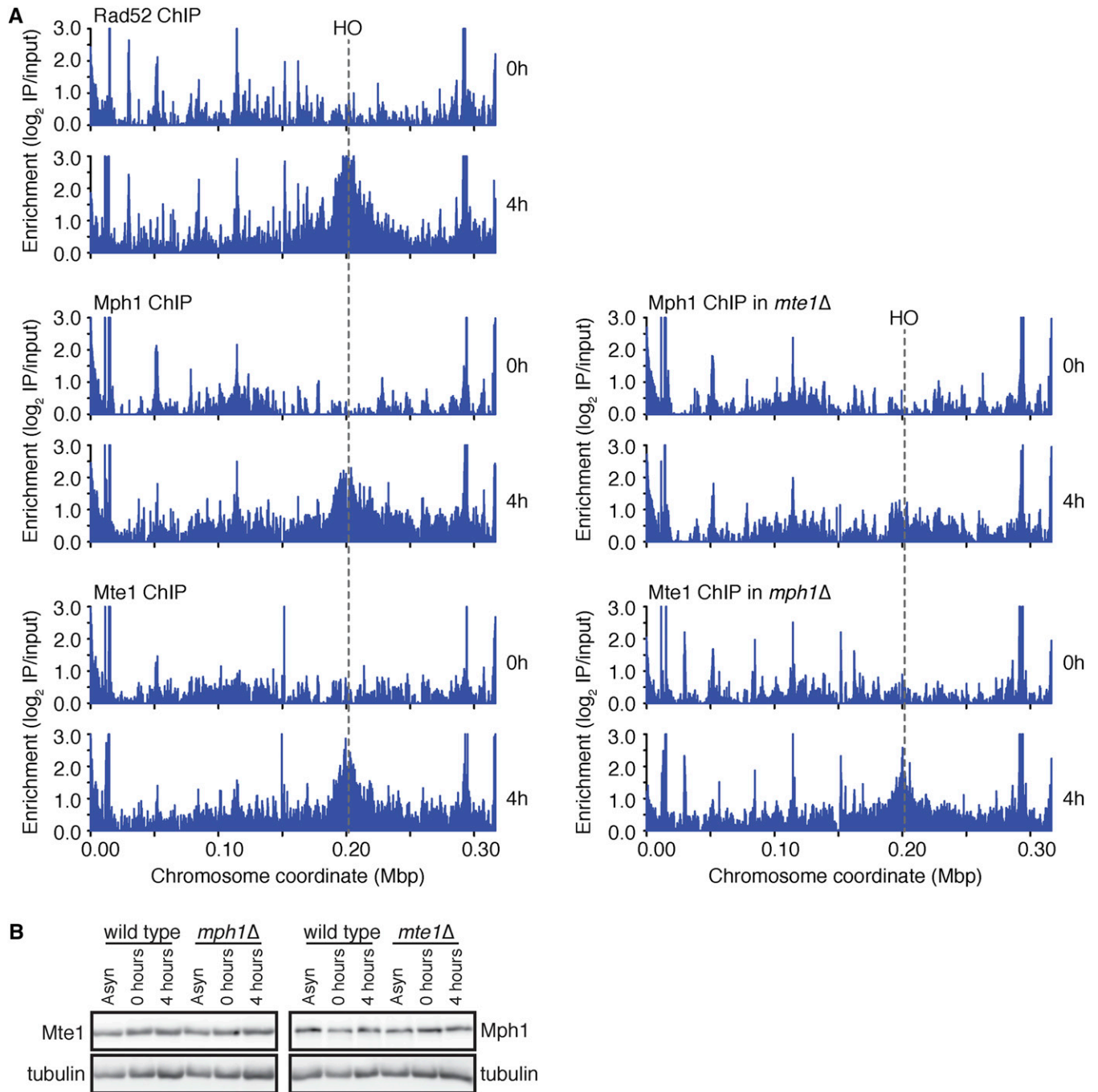


Figure 5 Mte1 and Mph1 are recruited to double-strand DNA breaks. (A) ChIP-seq analysis was performed on *RAD52-FLAG*, *MTE1-FLAG*, *MTE1-FLAG mph1Δ*, *MPH1-FLAG*, and *MPH1-FLAG mte1Δ* cells at 0 hr and 4 hr following the induction of a specific irreparable double-strand break at the *MAT* locus by the HO endonuclease. ChIP enrichment scores representing the \log_2 immunoprecipitate to input ratio are plotted across chromosome III for each time point. The position of the HO cut site is indicated by a dashed line. (B) Extracts from cells used in A were subjected to immunoblot analysis and probed with an antiflag antibody and an antitubulin antibody (as a loading control).

telomere maintenance protein). Thus, we now refer to *YGR042W* as *MTE1*.

***Mte1* foci form in S/G2 phase and in response to double-strand breaks**

The foci formed by Mte1 in response to phleomycin localize to the nucleus (Figure 2A) and form more frequently in cells in S

and G2 phases than in G1 cells (Figure 2B). Mte1 foci also form in the absence of DNA damaging agents, in 13% of cells during S or G2 phase, but in only 3% of cells during G1 phase (Figure 2B), similar to Rad52 foci (Lisby *et al.* 2001). As expected, Mte1 foci levels increase with increasing phleomycin concentration and with increasing time of phleomycin exposure (Figure 2C). Deletion of *MTE1* confers modest

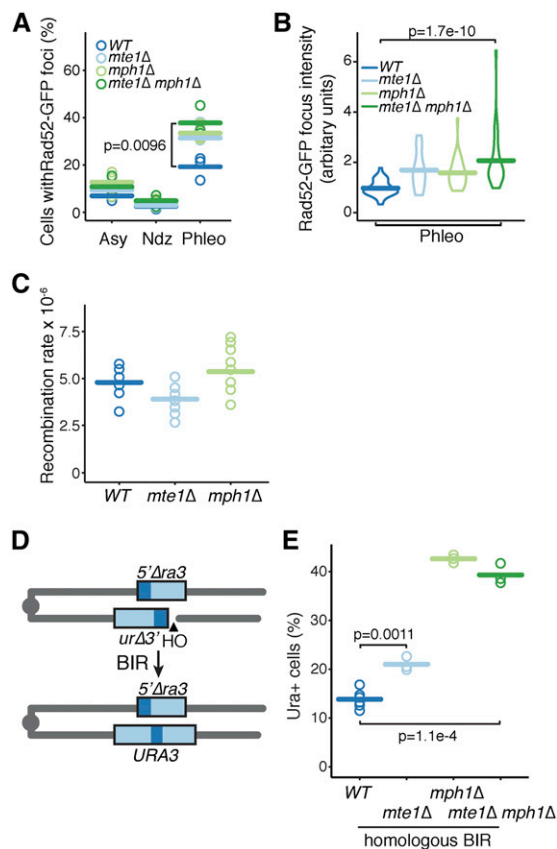


Figure 6 *MTE1* contributes to double-strand break repair. (A) The percent of cells with Rad52 foci is plotted for the indicated strains. Samples were from logarithmic phase (Asy), G2/M (NdZ), and after treatment with 50 $\mu\text{g/ml}$ phleomycin for 30 min (Phleo). Three replicates for each strain, for each condition, are plotted. The bars show the mean of the three replicates. *N* ranged from 42 to 160 cells per strain per replicate. The indicated samples were compared using a one-sided *t*-test. (B) The distribution of Rad52 focus intensity is plotted for the indicated strains, after treatment with 50 $\mu\text{g/ml}$ phleomycin for 30 min (Phleo). The width of the box indicates the number of foci with a given intensity, and the bar indicates the mean. *N* = 30 for all samples. The distributions were compared using the Wilcoxon rank sum test. (C) The direct repeat recombination rate (events/cell/generation) was measured for the indicated strains. Each assay was a fluctuation test of nine cultures. The bars show the means of 10 replicates. (D) Schematic of the strain used to measure BIR. A DSB is induced by expression of the *HO* endonuclease gene. The right arm of chromosome III invades the left arm, and replication restores a functional *URA3* gene. (E) BIR was quantified for wild-type, *mte1Δ*, *mph1Δ*, and *mte1Δ mph1Δ* strains. *N* ranged from 3 to 6. The bars show the means of the replicates, and strains were compared using a *t*-test.

sensitivity to phleomycin, but not to other DNA damaging and replication stress agents, methyl methanesulfonate, hydroxyurea, and camptothecin (Figure 2D).

Mte1* foci are increased when end resection is defective and depend on *MPH1

We tested whether *Mte1* focus formation was altered in mutants of genes encoding other proteins that form nuclear foci. Of 52 mutants tested, 5 led to increased *Mte1* focus formation (Figure 3A and Table S6). Three of the mutants, in *MRE11*, *RAD50*, and *XRS2*, would eliminate the DSB

end-resection function of the MRX complex (Ivanov *et al.* 1994), and *RAD52* is critical for formation of the Rad51 filament at resected DSBs (Sugawara *et al.* 2003), among other functions. *Mte1* foci increase in both the presence and absence of phleomycin in *mre11Δ*, *rad50Δ*, *xrs2Δ*, and *rad52Δ*, indicating that spontaneous DSBs are either more prevalent in these mutants or are repaired less effectively. By contrast, the *rad9Δ* mutant, which is defective in DNA damage checkpoint signaling and results in faster end resection at a double-strand break (Lazzaro *et al.* 2008; Ferrari *et al.* 2015), displays increased *Mte1* foci only in the presence of phleomycin. We tested whether other checkpoint mutants result in increased *Mte1* foci (Figure 3A). We disrupted checkpoint signaling upstream of Rad9 by deleting *MEC1*, *TEL1*, or both, and found that only the *mec1Δ tel1Δ* double mutant had a statistically evident increase in *Mte1* foci, in both the absence and presence of phleomycin ($P = 5.2 \times 10^{-5}$ and $P = 0.00095$, one-sided *t*-test). Interestingly, *mec1Δ tel1Δ* cells, like *rad9Δ*, have a higher rate of resection (Tsabar *et al.* 2015), and so increased *Mte1* foci in these mutants could reflect increased resection of the DSB.

Two mutants, *mph1Δ* and *rpa2-ph* (a temperature-sensitive allele of *RPA2*), caused decreased *Mte1* focus formation (Figure 3B). Interestingly, *Mph1* and *RPA* are proposed to function together to suppress recombination (Banerjee *et al.* 2008), and so perhaps the effect of *rpa2-ph* is indirect via *Mph1* recruitment. *Mph1* forms nuclear foci in unperturbed cells and in MMS (Chen *et al.* 2009), and we find that *Mph1* foci increase in the presence of phleomycin (Figure 3C). Deletion of *MTE1* reduces *Mph1* foci to background levels (Figure 3C), suggesting that *Mph1* and *Mte1* might function in concert.

***Mte1* and *Mph1* interact physically and are in the same genetic pathway**

We tested whether *Mte1* interacts with *Mph1* in coimmunoprecipitation experiments (Figure 4). We found that *Mte1* immunoprecipitates contain *Mph1* (Figure 4A), and that *Mph1* immunoprecipitates contain *Mte1* (Figure 4B). *Mte1* and *Mph1* appear to interact constitutively, as the extent of coimmunoprecipitation is unaffected by the presence of phleomycin. Consistent with *Mte1* and *Mph1* forming a complex, 38% of *Mte1* foci colocalize with *Mph1* after 3 hr in phleomycin (Figure 4C). Both *mte1Δ* and *mph1Δ* confer modest sensitivity to phleomycin, and the double mutant *mte1Δ mph1Δ* is no more sensitive than either of the single mutants, suggesting the *MTE1* and *MPH1* function in the same genetic DSB response pathway. By contrast, *mte1Δ* and *rad52Δ* show additive phleomycin sensitivity (Figure 4D), indicating that *MTE1* and *RAD52* play nonredundant roles in DSB repair.

***Mte1* and *Mph1* localize to double-strand DNA breaks**

Many proteins involved in double-strand DNA break repair are physically associated with chromatin adjacent to strand breaks *in vivo*, including *Mph1* (Prakash *et al.* 2009). We used chromatin immunoprecipitation followed by deep

sequencing to assess binding of Mte1 and Mph1 to the region flanking an induced HO double-strand break (Figure 5). The HO double-strand break was induced by growth in galactose to induce expression of the *HO* endonuclease gene. Cultures were sampled before *HO* induction, and after 4 hr in galactose, cross-linked with formaldehyde, and subjected to chromatin immunoprecipitation. Enrichment of DNA sequences in the immunoprecipitate relative to the input sample indicates regions of protein binding. We first tested Rad52, which is known to localize robustly to DSBs *in vivo* (Wolner *et al.* 2003), and found a peak of enrichment on chromosome III following *HO* induction, centered on the HO endonuclease site (Figure 5A). Similar peaks were detected at the induced DSB for both Mte1 and Mph1, indicating that the Mte1–Mph1 protein complex is recruited to DNA double-strand breaks *in vivo* (Figure 5A). Of particular interest, Mph1 enrichment at the DSB was reduced in an *mte1Δ* mutant, and Mte1 enrichment at the DSB was reduced (although to a lesser extent) in an *mph1Δ* mutant (Figure 5A). Mte1 and Mph1 protein levels were unchanged in the mutant backgrounds (Figure 5B), suggesting that the functional unit recruited to DSBs is an Mte1–Mph1 complex.

Increased phleomycin-induced DSBs in the absence of MTE1

The presence of Mte1 at an induced DSB, and the sensitivity of *mte1Δ* strains to DSBs, suggested that Mte1 could play a role in DSB repair. We measured Rad52 focus formation as a proxy for the presence of DNA damage. Cells were blocked in G2 phase with nocodazole and treated with 50 μg/ml phleomycin for 30 min. Phleomycin caused an increase in the fraction of cells with Rad52 foci in *mph1Δ*, *mte1Δ*, and the *mph1Δ mte1Δ* double mutant compared to the wild type (Figure 6A) and an increase in Rad52 focus intensity (Figure 6B). The *mph1Δ* and *mte1Δ* single mutants and the *mph1Δ mte1Δ* double mutant had similar effects in both assays, suggesting that *MTE1* and *MPH1* function together in DSB repair. We measured recombination directly in *mte1Δ* mutants (Figure 6C). In the absence of DNA damage, *mte1Δ*, like *mph1Δ* (Schurer *et al.* 2004), is proficient in mitotic recombination, displaying a recombination rate that is highly similar to the wild type.

MTE1 suppresses BIR

MPH1 suppresses BIR during double-strand break repair (Luke-Glaser and Luke 2012; Stafa *et al.* 2014). Given the physical and genetic interactions between Mte1 and Mph1 that our work has revealed, we tested whether *MTE1* also plays a role in suppressing BIR. We induced a DSB in strains carrying a modified chromosome V with a truncated *ura3* allele adjacent to an HO endonuclease site. Upon induction of the double-strand break, the truncated allele is repaired using donor sequences located on the other arm of chromosome V to yield Ura⁺ colonies (Figure 6D). In homologous BIR, where the sequences that recombine share 108 bp of homology, deletion of *mte1* results in increased BIR (Figure 6E).

Deletion of *mph1* also results in increased BIR (Figure 6E), as previously reported (Stafa *et al.* 2014). The double mutant *mph1Δ mte1Δ* displays increased BIR, much like *mph1Δ* (Figure 6E), indicating that *MPH1* and *MTE1* function in the same genetic pathway, and that *mph1Δ* is epistatic to *mte1Δ*. Since the magnitude of effect is greater in the *mph1Δ*, we infer that loss of *MTE1* only partially compromises *MPH1* function, consistent with reduced (but not eliminated) recruitment of Mph1 to DSBs in *mte1Δ* (Figure 5A). Together the data indicate that *MTE1*, like *MPH1*, is an important suppressor of BIR and therefore a suppressor of loss of heterozygosity.

Discussion

In response to DNA damage, most homologous recombination proteins are recruited to sites of double-strand DNA breaks. Among them, Rad52 is a key recombination protein and the Rad52 focus is considered to be a sensitive indicator of DNA repair (Lisby *et al.* 2001, 2003; Alvaro *et al.* 2007). We identified 29 proteins that localize to Rad52 foci in response to DNA damage. Among them, we identified a role for *YGR042W/MTE1* in DNA double-strand break repair. Similar to many DNA repair proteins, Mte1 forms nuclear foci in response to double-strand breaks, and Mte1 foci only form when the DNA helicase Mph1 is present. Mte1 forms protein complexes with Mph1, and both proteins are recruited to the chromatin flanking double-strand DNA breaks *in vivo*. In the absence of *MTE1* the Rad52 repair centers accumulate, and *MTE1* is important for suppressing break-induced replication. Together our data indicate that Mph1 function in recombination repair of double-strand breaks requires Mte1.

How does Mte1 impact Mph1 function?

Mte1 and Mph1 appear to be members of a constitutive complex. The interaction between these two proteins, whether direct or indirect, was readily detected by coimmunoprecipitation of either protein even in the absence of DNA damage. Mte1 is important for Mph1 nuclear focus formation, and more importantly, for recruitment of Mph1 to double-strand breaks *in vivo*. These data suggest that Mph1 functions as part of a protein complex containing Mte1. Consistent with this notion, deletion of *MTE1* conferred sensitivity to phleomycin that was similar to that conferred by deletion of *MPH1*, and the *mte1Δ mph1Δ* double mutant was no more sensitive, indicating that these genes function in the same genetic pathway for phleomycin resistance.

Our data suggest that Mte1 is not simply a structural component of Mph1 complexes, as Mte1 appears to have little effect on Mph1 stability *in vivo*. Mte1 could presumably play a role in targeting Mph1 to specific substrates *in vivo*. Such a role would be consistent with our findings that Mph1 nuclear foci and recruitment or retention of Mph1 at double-strand breaks is compromised when *MTE1* is absent. *MPH1* suppresses crossovers and BIR by unwinding D-loop recombination intermediates (Prakash *et al.* 2009; Mazon and

Symington 2013; Stafa *et al.* 2014). We find that *MTE1* suppresses BIR much like *MPH1*, thus it is also possible that Mte1 facilitates some aspect of Mph1 catalysis. Mte1 lacks obvious catalytic domains, and purified Mph1 is capable of unwinding D-loops and extended D-loops *in vitro* in the absence of Mte1 (Sun *et al.* 2008; Prakash *et al.* 2009; Sebesta *et al.* 2011). Nonetheless, it will be of great interest to determine whether Mte1 modulates Mph1 activity *in vitro*, as it appears that *in vivo* Mph1 is normally assembled into complexes that contain Mte1.

Orthologs of *MTE1*

MTE1 has readily identifiable orthologs in other yeasts, including *Kluyveromyces*, *Candida*, *Pichia*, and *Ashbya* species. *MTE1* appears to be an ortholog of the *Schizosaccharomyces pombe* *dbl2⁺* gene (Yu *et al.* 2013). *Db12* colocalizes with the fission yeast Rad52, and with double-strand breaks, and is important for nuclear focus formation by Fml1, the fission yeast ortholog of Mph1 (Yu *et al.* 2013). *dbl2⁺* does not have a clear role in *fml1⁺* inhibition of crossovers or inhibition of BIR as of yet, so it is not known if *dbl2⁺* plays a functional role similar to *MTE1*. Mte1 contains a domain of unknown function, DUF2439, which is found in the human ZGRF1 protein. The DUF2439 domain is also found in *Db12* (Yu *et al.* 2013), but does not appear to be important for DNA damage resistance or for nuclear focus formation. Further, ZGRF1 is likely membrane anchored and so might not be a true ortholog of Mte1. Nonetheless, as several lines of evidence suggest that Mph1 is an ortholog of the human FANCM protein (Whitby 2010; Xue *et al.* 2015), our evidence that Mph1 functions in concert with an important cofactor is consistent with modulation of diverse FANCM activities by different binding partners in metazoans (Ciccina *et al.* 2007; Deans and West 2009; Singh *et al.* 2010; Yan *et al.* 2010; Leung *et al.* 2012; Yan *et al.* 2012). It will be of interest to determine how Mte1 modulates Mph1 function, and whether FANCM is similarly regulated.

Acknowledgments

We thank members of the laboratories of Brenda Andrews and Charlie Boone for assistance with microscopy and Tobit Glenhaber and Linus Glenhaber for assistance in constructing *mte1* deletion strains to measure BIR efficiency. We also thank Lorraine Symington and Daniel Durocher for providing strains and Patrick Sung, Michael Lisby, and Lorraine Symington for sharing data prior to publication. This work was supported by grants from the Canadian Cancer Society Research Institute (impact grant 702310 to G.W.B.), the Cancer Research Society (G.W.B.), the Natural Sciences and Engineering Research Council of Canada (discovery grant 327612 to Z.Z.), and the National Institutes of Health (GM76020 to J.E.H.).

Author contributions: A.Y. designed and carried out the experiments, wrote the paper, and edited the paper; T.K.

analyzed ChIP-seq data and edited the paper; R.P.A. performed and analyzed BIR assays; S.M. performed recombination assays and edited the paper; J.O. performed recombination analysis and constructed strains; J.E.H. edited the paper; Z.Z. analyzed ChIP-seq data and edited the paper; and G.W.B. designed the experiments, wrote the paper, and edited the paper. The authors declare that they have no conflict of interest.

Literature Cited

- Alvaro, D., M. Lisby, and R. Rothstein, 2007 Genome-wide analysis of Rad52 foci reveals diverse mechanisms impacting recombination. *PLoS Genet.* 3: e228.
- Anand, R. P., O. Tsaponina, P. W. Greenwell, C. S. Lee, W. Du *et al.*, 2014 Chromosome rearrangements via template switching between diverged repeated sequences. *Genes Dev.* 28: 2394–2406.
- Askree, S. H., T. Yehuda, S. Smolikov, R. Gurevich, J. Hawk *et al.*, 2004 A genome-wide screen for *Saccharomyces cerevisiae* deletion mutants that affect telomere length. *Proc. Natl. Acad. Sci. USA* 101: 8658–8663.
- Balint, A., T. Kim, D. Gallo, J. R. Cussiol, F. M. Bastos de Oliveira *et al.*, 2015 Assembly of Slx4 signaling complexes behind DNA replication forks. *EMBO J.* 34: 2182–2197.
- Banerjee, S., S. Smith, J. H. Oum, H. J. Liaw, J. Y. Hwang *et al.*, 2008 Mph1p promotes gross chromosomal rearrangement through partial inhibition of homologous recombination. *J. Cell Biol.* 181: 1083–1093.
- Blanco, M. G., J. Matos, U. Rass, S. C. Ip, and S. C. West, 2010 Functional overlap between the structure-specific nucleases Yen1 and Mus81-Mms4 for DNA-damage repair in *S. cerevisiae*. *DNA Repair (Amst.)* 9: 394–402.
- Brachmann, C. B., A. Davies, G. J. Cost, E. Caputo, J. Li *et al.*, 1998 Designer deletion strains derived from *Saccharomyces cerevisiae* S288C: a useful set of strains and plasmids for PCR-mediated gene disruption and other applications. *Yeast* 14: 115–132.
- Burgess, R. C., M. Lisby, V. Altmannova, L. Krejci, P. Sung *et al.*, 2009 Localization of recombination proteins and Srs2 reveals anti-recombinase function *in vivo*. *J. Cell Biol.* 185: 969–981.
- Chavez, A., V. Agrawal, and F. B. Johnson, 2011 Homologous recombination-dependent rescue of deficiency in the structural maintenance of chromosomes (Smc) 5/6 complex. *J. Biol. Chem.* 286: 5119–5125.
- Chen, Y. H., K. Choi, B. Szakal, J. Arenz, X. Duan *et al.*, 2009 Interplay between the Smc5/6 complex and the Mph1 helicase in recombinational repair. *Proc. Natl. Acad. Sci. USA* 106: 21252–21257.
- Chen, Y. H., B. Szakal, F. Castellucci, D. Branzei, and X. Zhao, 2013 DNA damage checkpoint and recombinational repair differentially affect the replication stress tolerance of Smc6 mutants. *Mol. Biol. Cell* 24: 2431–2441.
- Cherry, J. M., E. L. Hong, C. Amundsen, R. Balakrishnan, G. Binkley *et al.*, 2012 *Saccharomyces* Genome Database: the genomics resource of budding yeast. *Nucleic Acids Res.* 40: D700–D705.
- Choi, K., B. Szakal, Y. H. Chen, D. Branzei, and X. Zhao, 2010 The Smc5/6 complex and Esc2 influence multiple replication-associated recombination processes in *Saccharomyces cerevisiae*. *Mol. Biol. Cell* 21: 2306–2314.
- Ciccina, A., C. Ling, R. Coulthard, Z. Yan, and Y. Xue *et al.*, 2007 Identification of FAAP24, a Fanconi anemia core complex protein that interacts with FANCM. *Mol. Cell* 25: 331–343.
- Deans, A. J., and S. C. West, 2009 FANCM connects the genome instability disorders Bloom's Syndrome and Fanconi Anemia. *Mol. Cell* 36: 943–953.

- Denervaud, N., J. Becker, R. Delgado-Gonzalo, P. Damay, A. S. Rajkumar *et al.*, 2013 A chemostat array enables the spatio-temporal analysis of the yeast proteome. *Proc. Natl. Acad. Sci. USA* 110: 15842–15847.
- Engel, S. R., F. S. Dietrich, D. G. Fisk, G. Binkley, R. Balakrishnan *et al.*, 2014 The reference genome sequence of *Saccharomyces cerevisiae*: then and now. *G3 (Bethesda)* 4: 389–398.
- Entian, K. D., T. Schuster, J. H. Hegemann, D. Becher, H. Feldmann *et al.*, 1999 Functional analysis of 150 deletion mutants in *Saccharomyces cerevisiae* by a systematic approach. *Mol. Gen. Genet.* 262: 683–702.
- Ferrari, M., D. Dibitetto, G. De Gregorio, V. V. Eapen, C. C. Rawal *et al.*, 2015 Functional interplay between the 53BP1-ortholog Rad9 and the Mre11 complex regulates resection, end-tethering and repair of a double-strand break. *PLoS Genet.* 11: e1004928.
- Gallina, I., C. Colding, P. Henriksen, P. Beli, K. Nakamura *et al.*, 2015 Cmr1/WDR76 defines a nuclear genotoxic stress body linking genome integrity and protein quality control. *Nat. Commun.* 6: 6533.
- Germann, S. M., V. H. Oestergaard, C. Haas, P. Salis, A. Motegi *et al.*, 2011 Dpb11/TopBP1 plays distinct roles in DNA replication, checkpoint response and homologous recombination. *DNA Repair (Amst.)* 10: 210–224.
- Ho, C. K., G. Mazon, A. F. Lam, and L. S. Symington, 2010 Mus81 and Yen1 promote reciprocal exchange during mitotic recombination to maintain genome integrity in budding yeast. *Mol. Cell* 40: 988–1000.
- Huh, W. K., J. V. Falvo, L. C. Gerke, A. S. Carroll, R. W. Howson *et al.*, 2003 Global analysis of protein localization in budding yeast. *Nature* 425: 686–691.
- Ivanov, E. L., N. Sugawara, C. I. White, F. Fabre, and J. E. Haber, 1994 Mutations in *XRS2* and *RAD50* delay but do not prevent mating-type switching in *Saccharomyces cerevisiae*. *Mol. Cell Biol.* 14: 3414–3425.
- Kee, Y., and A. D. D'Andrea, 2010 Expanded roles of the Fanconi anemia pathway in preserving genomic stability. *Genes Dev.* 24: 1680–1694.
- Langmead, B., and S. L. Salzberg, 2012 Fast gapped-read alignment with Bowtie 2. *Nat. Methods* 9: 357–359.
- Lazzaro, F., V. Sapountzi, M. Granata, A. Pellicoli, M. Vaze *et al.*, 2008 Histone methyltransferase Dot1 and Rad9 inhibit single-stranded DNA accumulation at DSBs and uncapped telomeres. *EMBO J.* 27: 1502–1512.
- Lea, D. E., and C. A. Coulson, 1949 The distribution of the numbers of mutants in bacterial populations. *J. Genet.* 49: 264–285.
- Leung, J. W., Y. Wang, K. W. Fong, M. S. Huen, L. Li *et al.*, 2012 Fanconi anemia (FA) binding protein FAAP20 stabilizes FA complementation group A (FANCA) and participates in interstrand cross-link repair. *Proc. Natl. Acad. Sci. USA* 109: 4491–4496.
- Lisby, M., R. Rothstein, and U. H. Mortensen, 2001 Rad52 forms DNA repair and recombination centers during S phase. *Proc. Natl. Acad. Sci. USA* 98: 8276–8282.
- Lisby, M., U. H. Mortensen, and R. Rothstein, 2003 Colocalization of multiple DNA double-strand breaks at a single Rad52 repair centre. *Nat. Cell Biol.* 5: 572–577.
- Lisby, M., J. H. Barlow, R. C. Burgess, and R. Rothstein, 2004 Choreography of the DNA damage response; spatiotemporal relationships among checkpoint and repair proteins. *Cell* 118: 699–713.
- Luke-Glaser, S., and B. Luke, 2012 The Mph1 helicase can promote telomere uncapping and premature senescence in budding yeast. *PLoS One* 7: e42028.
- Mazon, G., and L. S. Symington, 2013 Mph1 and Mus81-Mms4 prevent aberrant processing of mitotic recombination intermediates. *Mol. Cell* 52: 63–74.
- Mazumder, A., L. Q. Pesudo, S. McRee, M. Bathe, and L. D. Samson, 2013 Genome-wide single-cell-level screen for protein abundance and localization changes in response to DNA damage in *S. cerevisiae*. *Nucleic Acids Res.* 41: 9310–9324.
- Melo, J. A., J. Cohen, and D. P. Toczyski, 2001 Two checkpoint complexes are independently recruited to sites of DNA damage *in vivo*. *Genes Dev.* 15: 2809–2821.
- Pellicoli, A., C. Lucca, G. Liberi, F. Marini, M. Lopes *et al.*, 1999 Activation of Rad53 kinase in response to DNA damage and its effect in modulating phosphorylation of the lagging strand DNA polymerase. *EMBO J.* 18: 6561–6572.
- Prakash, R., L. Krejci, S. Van Komen, K. Anke Schurer, W. Kramer *et al.*, 2005 *Saccharomyces cerevisiae* *MPH1* gene, required for homologous recombination-mediated mutation avoidance, encodes a 3' to 5' DNA helicase. *J. Biol. Chem.* 280: 7854–7860.
- Prakash, R., D. Satory, E. Dray, A. Papusha, J. Scheller *et al.*, 2009 Yeast Mph1 helicase dissociates Rad51-made D-loops: implications for crossover control in mitotic recombination. *Genes Dev.* 23: 67–79.
- Roberts, T. M., I. W. Zaidi, J. A. Vaisica, M. Peter, and G. W. Brown, 2008 Regulation of Rtt107 recruitment to stalled DNA replication forks by the cullin Rtt101 and the Rtt109 acetyltransferase. *Mol. Biol. Cell* 19: 171–180.
- Scheller, J., A. Schurer, C. Rudolph, S. Hettwer, and W. Kramer, 2000 *MPH1*, a yeast gene encoding a DEAH protein, plays a role in protection of the genome from spontaneous and chemically induced damage. *Genetics* 155: 1069–1081.
- Schurer, K. A., C. Rudolph, H. D. Ulrich, and W. Kramer, 2004 Yeast *MPH1* gene functions in an error-free DNA damage bypass pathway that requires genes from Homologous recombination, but not from postreplicative repair. *Genetics* 166: 1673–1686.
- Sebesta, M., P. Burkovics, L. Haracska, and L. Krejci, 2011 Reconstitution of DNA repair synthesis *in vitro* and the role of polymerase and helicase activities. *DNA Repair (Amst.)* 10: 567–576.
- Shimomura, T., S. Ando, K. Matsumoto, and K. Sugimoto, 1998 Functional and physical interaction between Rad24 and Rfc5 in the yeast checkpoint pathways. *Mol. Cell Biol.* 18: 5485–5491.
- Singh, T. R., D. Saro, A. M. Ali, X. F. Zheng, C. H. Du *et al.*, 2010 MHF1–MHF2, a histone-fold-containing protein complex, participates in the Fanconi anemia pathway via FANCM. *Mol. Cell* 37: 879–886.
- Smith, J., and R. Rothstein, 1999 An allele of *RFA1* suppresses *RAD52*-dependent double-strand break repair in *Saccharomyces cerevisiae*. *Genetics* 151: 447–458.
- Stafa, A., R. A. Donnianni, L. A. Timashev, A. F. Lam, and L. S. Symington, 2014 Template switching during break-induced replication is promoted by the Mph1 helicase in *Saccharomyces cerevisiae*. *Genetics* 196: 1017–1028.
- Sugawara, N., X. Wang, and J. E. Haber, 2003 *In vivo* roles of Rad52, Rad54, and Rad55 proteins in Rad51-mediated recombination. *Mol. Cell* 12: 209–219.
- Sun, W., S. Nandi, F. Osman, J. S. Ahn, J. Jakovleska *et al.*, 2008 The FANCM ortholog Fml1 promotes recombination at stalled replication forks and limits crossing over during DNA double-strand break repair. *Mol. Cell* 32: 118–128.
- Symington, L. S., 2002 Role of *RAD52* epistasis group genes in homologous recombination and double-strand break repair. *Microbiol. Mol. Biol. Rev.* 66: 630–670, table of contents.
- Szostak, J. W., T. L. Orr-Weaver, R. J. Rothstein, and F. W. Stahl, 1983 The double-strand-break repair model for recombination. *Cell* 33: 25–35.
- Tkach, J. M., A. Yimit, A. Y. Lee, M. Riffle, M. Costanzo *et al.*, 2012 Dissecting DNA damage response pathways by analysing

- protein localization and abundance changes during DNA replication stress. *Nat. Cell Biol.* 14: 966–976.
- Tsabar, M., V. V. Eapen, J. M. Mason, G. Memisoglu, D. P. Waterman *et al.*, 2015 Caffeine impairs resection during DNA break repair by reducing the levels of nucleases Sae2 and Dna2. *Nucleic Acids Res.* 43: 6889–6901.
- Whitby, M. C., 2010 The FANCM family of DNA helicases/translocases. *DNA Repair (Amst.)* 9: 224–236.
- Wolner, B., S. van Komen, P. Sung, and C. L. Peterson, 2003 Recruitment of the recombinational repair machinery to a DNA double-strand break in yeast. *Mol. Cell* 12: 221–232.
- Wu, L., and I. D. Hickson, 2003 The Bloom's syndrome helicase suppresses crossing over during homologous recombination. *Nature* 426: 870–874.
- Wu, L., C. Z. Bachrati, J. Ou, C. Xu, J. Yin *et al.*, 2006 BLAP75/RMI1 promotes the BLM-dependent dissolution of homologous recombination intermediates. *Proc. Natl. Acad. Sci. USA* 103: 4068–4073.
- Xue, X., K. Choi, J. Bonner, T. Chiba, Y. Kwon *et al.*, 2014 Restriction of replication fork regression activities by a conserved SMC complex. *Mol. Cell* 56: 436–445.
- Xue, X., P. Sung, and X. Zhao, 2015 Functions and regulation of the multitasking FANCM family of DNA motor proteins. *Genes Dev.* 29: 1777–1788.
- Yan, Z., M. Delannoy, C. Ling, D. Dae, F. Osman *et al.*, 2010 A histone-fold complex and FANCM form a conserved DNA-remodeling complex to maintain genome stability. *Mol. Cell* 37: 865–878.
- Yan, Z., R. Guo, M. Paramasivam, W. Shen, C. Ling *et al.*, 2012 A ubiquitin-binding protein, FAAP20, links RNF8-mediated ubiquitination to the Fanconi anemia DNA repair network. *Mol. Cell* 47: 61–75.
- Yang, J., C. Z. Bachrati, J. Ou, I. D. Hickson, and G. W. Brown, 2010 Human topoisomerase IIIalpha is a single-stranded DNA decatenase that is stimulated by BLM and RMI1. *J. Biol. Chem.* 285: 21426–21436.
- Yu, Y., J. Y. Ren, J. M. Zhang, F. Suo, X. F. Fang *et al.*, 2013 A proteome-wide visual screen identifies fission yeast proteins localizing to DNA double-strand breaks. *DNA Repair (Amst.)* 12: 433–443.
- Zheng, X. F., R. Prakash, D. Saro, S. Longerich, H. Niu *et al.*, 2011 Processing of DNA structures via DNA unwinding and branch migration by the *S. cerevisiae* Mph1 protein. *DNA Repair (Amst.)* 10: 1034–1043.
- Zhu, Z., W. H. Chung, E. Y. Shim, S. E. Lee, and G. Ira, 2008 Sgs1 helicase and two nucleases Dna2 and Exo1 resect DNA double-strand break ends. *Cell* 134: 981–994.

Communicating editor: N. M. Hollingsworth

GENETICS

Supporting Information

www.genetics.org/lookup/suppl/doi:10.1534/genetics.115.185454/-/DC1

***MTE1* Functions with *MPH1* in Double-Strand Break Repair**

Askar Yimit, TaeHyung Kim, Ranjith P. Anand, Sarah Meister, Jiongwen Ou, James E. Haber,
Zhaolei Zhang, and Grant W. Brown

Table S1. Yeast Strains used in this study.

Strain	Genotype	Source
GFP collection	<i>MATa xxx-GFP::HIS3MX ura3Δ0 leu2Δ0 his3Δ1 met15Δ0</i>	Huh et al, 2003
AYY38	<i>MATα RAD52-yEmRFP::CaURA3 can1 Δ::STE2pr-LEU2 leu2Δ0 his3Δ1 ura3Δ0 met15Δ0 lyp1 Δ</i>	this study
AYY110	<i>MATα MTEI-GFP::HIS3MX can1 Δ::STE2pr-LEU2 NUP49-mCherry::CaURA3 leu2Δ0 his3Δ1 ura3Δ0 met15Δ0 lyp1 Δ</i>	this study
GBY717	<i>MATa mte1 Δ::kanMX ura3Δ0 leu2Δ0 his3Δ1 met15Δ0 lys2Δ0</i>	this study
Deletion collection	<i>MATa xxx::kanMX ura3Δ0 leu2Δ0 his3Δ1 met15Δ0</i>	Giaever et al, 2002
AYY73	<i>MATa MTEI-GFP::kanMX ura3Δ0 leu2Δ0 his3Δ1 met15Δ0</i>	this study
AYY56	<i>MATa MTEI-GFP::HIS3MX mec1 Δ::LEU2 smf1 Δ::kanMX leu2Δ0 his3Δ1 ura3Δ0 met15Δ0</i>	this study
AYY57	<i>MATa MTEI-GFP::HIS3MX tell Δ::natMX leu2Δ0 his3Δ1 ura3Δ0</i>	this study
AYY76	<i>MATa MTEI-GFP::HIS3MX mec1 Δ::LEU2 tell Δ::natMX smf1 Δ::kanMX leu2Δ0 his3Δ1 ura3Δ0</i>	this study
	<i>MATa MTEI-GFP::kanMX rad52Δ::natMX leu2Δ0 his3Δ1 ura3Δ0 met15Δ0 can1 Δ::STE2pr-LEU2</i>	this study
	<i>MATa MTEI-GFP::kanMX mre11 Δ::natMX leu2Δ0 his3Δ1 ura3Δ0 met15Δ0 can1 Δ::STE2pr-LEU2</i>	this study
	<i>MATa MTEI-GFP::kanMX rad50Δ::natMX leu2Δ0 his3Δ1 ura3Δ0 met15Δ0 can1 Δ::STE2pr-LEU2</i>	this study
	<i>MATa MTEI-GFP::kanMX xrs2Δ::natMX leu2Δ0 his3Δ1 ura3Δ0 met15Δ0 can1 Δ::STE2pr-LEU2</i>	this study
	<i>MATa MTEI-GFP::kanMX rad9Δ::natMX leu2Δ0 his3Δ1 ura3Δ0 met15Δ0 can1 Δ::STE2pr-LEU2</i>	this study
	<i>MATa MTEI-GFP::kanMX mph1 Δ::natMX ura3Δ0 leu2Δ0 his3Δ1 met15Δ0 can1 Δ::STE2pr-LEU2</i>	this study
Y1429	<i>MATα rfa2-ph::natMX can1 Δ::STE2pr-Sphis5 leu2Δ0 his3Δ1 ura3Δ0 met15Δ0 lyp1 Δ</i>	C. Boone
	<i>MATa MTEI-GFP::kanMX mgs1 Δ::natMX leu2Δ0 his3Δ1 ura3Δ0 met15Δ0</i>	this study
	<i>MATa MTEI-GFP::kanMX rfa2-ph::natMX leu2Δ0 his3Δ1 ura3Δ0 met15Δ0</i>	this study
AYY85	<i>MATa MPH1-GFP::HIS3MX ura3Δ0 leu2Δ0 his3Δ1 met15Δ0</i>	this study
AYY107	<i>MATa MPH1-GFP::HIS3MX mte1 Δ::kanMX can1 Δ::STE2pr-LEU2 RPL39pr-TdTomato::CaURA3 leu2Δ0 his3Δ1 ura3Δ0 lyp1 Δ</i>	this study
AYY75	<i>MATa MTEI-6His10flag::kanMX ura3Δ0 leu2Δ0 his3Δ1 met15Δ0</i>	this study
AYY139	<i>MATa MPH1-3HA::HIS3MX MTEI-6His10flag::kanMX his3Δ1 leuΔ0 ura3Δ0 met15Δ0</i>	this study
GBY708	<i>MATa hoΔ::kanMX ura3Δ0 leu2Δ0 his3Δ1 met15Δ0</i>	this study
GBY713	<i>MATa mte1 Δ::kanMX rad52Δ::kanMX leu2Δ0 his3Δ1 ura3Δ0 met15Δ0</i>	this study
GBY719	<i>MATa mte1 Δ::kanMX mph1 Δ::kanMX leu2Δ0 his3Δ1 ura3Δ0 met15Δ0 lys2Δ0</i>	this study
GBY706	<i>MATa rad52Δ::kanMX leu2Δ0 his3Δ1 ura3Δ0 met15Δ0</i>	this study
GBY716	<i>MATa mph1 Δ::kanMX leu2Δ0 his3Δ1 ura3Δ0 met15Δ0</i>	this study
AYY182	<i>MATα RAD52-6His10flag::kanMX hoΔ hmlΔ::ADE1 hmrΔ::ADE1 ade1 leu2-3,112 trp1::hisG lys5 ura3-52 ade3::GAL1pr-HO</i>	this study
AYY140	<i>MATα MTEI-6His10flag::kanMX hoΔ hmlΔ::ADE1 hmrΔ::ADE1 ade1 leu2-3,112 trp1::hisG lys5 ura3-52 ade3::GAL1pr-HO</i>	this study
AYY148	<i>MATα MTEI-6His10flag::kanMX mph1 Δ::natMX hoΔ hmlΔ::ADE1 hmrΔ::ADE1 ade1 leu2-3,112 trp1::hisG lys5 ura3-52 ade3::GAL1pr-HO</i>	this study
AYY156	<i>MATα MPH1-6His10flag::kanMX hoΔ hmlΔ::ADE1 hmrΔ::ADE1 ade1 leu2-3,112 trp1::hisG lys5 ura3-52 ade3::GAL1pr-HO</i>	this study
AYY155	<i>MATα MPH1-6His10flag::kanMX mte1 Δ::natMX hoΔ hmlΔ::ADE1 hmrΔ::ADE1 ade1 leu2-3,112 trp1::hisG lys5 ura3-52 ade3::GAL1pr-HO</i>	this study
AYY116	<i>MATα RAD52-GFP::HIS3MX mte1 Δ::kanMX leu2Δ0 his3Δ1 ura3Δ0 lys2Δ0</i>	this study
AYY117	<i>MATα RAD52-GFP::HIS3MX mph1 Δ::natMX leu2Δ0 his3Δ1 ura3Δ0 lys2Δ0</i>	this study
AYY118	<i>MATα RAD52-GFP::HIS3MX mte1 Δ::kanMX mph1 Δ::natMX leu2Δ0 his3Δ1 ura3Δ0 lys2Δ0</i>	this study
JOY90	<i>MATα mfa1 Δ::MFA1pr-HIS3 leu2ΔEcoRI::URA3-HOcs::leu2ΔBstEII leu2Δ0 his3Δ1 ura3Δ0 met15Δ0 lyp1 Δ can1 Δ::natMX</i>	this study
AYY119	<i>MATα mte1 Δ::kanMX leu2ΔEcoRI::URA3-HOcs::leu2ΔBstEII leu2Δ0 his3Δ1 ura3Δ0 met15Δ0 lyp1 Δ can1 Δ::natMX</i>	this study
AYY120	<i>MATα mph1 Δ::kanMX leu2ΔEcoRI::URA3-HOcs::leu2ΔBstEII leu2Δ0 his3Δ1 ura3Δ0 met15Δ0 lyp1 Δ can1 Δ::natMX</i>	this study
yRA253	<i>MATαΔHOcs::hisG ura3Δ851 trp1Δ63 leu2Δ::kanMX hmlΔ::hisG hmrΔ::ADE3 ade3::GAL1pr-HO can1 Δ::URdonor-Hocs-natMX acceptorA3::TRP1</i>	this study
yRA276	<i>MATαΔHOcs::hisG ura3Δ851 trp1Δ63 leu2Δ::kanMX hmlΔ::hisG hmrΔ::ADE3 ade3::GAL1pr-HO can1 Δ::URdonor-Hocs-natMX acceptorA3::TRP1 mte1 Δ::LEU2MX</i>	this study
yRA281	<i>MATαΔHOcs::hisG ura3Δ851 trp1Δ63 leu2Δ::kanMX hmlΔ::hisG hmrΔ::ADE3 ade3::GAL1pr-HO can1 Δ::URdonor-Hocs-natMX acceptorA3::TRP1 mph1 Δ::hygMX</i>	this study
yRA286	<i>MATαΔHOcs::hisG ura3Δ851 trp1Δ63 leu2Δ::kanMX hmlΔ::hisG hmrΔ::ADE3 ade3::GAL1pr-HO can1 Δ::URdonor-Hocs-natMX acceptorA3::TRP1 mte1 Δ::LEU2MX mph1 Δ::hygMX</i>	this study
BY4741	<i>MATa ura3Δ0 leu2Δ0 his3Δ1 met15Δ0</i>	Brachmann et al. 1998

References

Brachmann CB, Davies A, Cost GJ, Caputo E, Li J, Hieter P, and Boeke JD (1998). Designer deletion strains derived from *Saccharomyces cerevisiae* S288C: a useful set of strains and plasmids for PCR-mediated gene disruption and other applications. *Yeast* **14**: 115-132.

Giaever G, Chu AM, Ni L, Connelly C, Riles L, Veronneau S, Dow S, Lucau-Danila A, Anderson K, Andre B, et al. (2002). Functional profiling of the *Saccharomyces cerevisiae* genome. *Nature* **418**: 387-391.

Huh WVK, Falvo JV, Gerke LC, Carroll AS, Howson RW, Weissman JS, and O'Shea EK (2003). Global analysis of protein localization in budding yeast. *Nature* **425**: 686-691.

Table S2. ChIP-seq statistics

Genotype	Strain	Condition	Sample Title	Sample Type	Sample Name	Sequencing Type	# of reads	Sequencing Coverage	Alignment Rate	SRA Accession Number
RAD52-FLAG	AYY182	0h + gal	15-06-10_1st_ay_w303_Rad52flag_WT_0h_input_S-50-H	Input	AY1	Single-end (50 bp)	18053040	73	97.18%	SRR2559330
RAD52-FLAG	AYY182	0h + gal	15-06-10_1st_ay_w303_Rad52flag_WT_0h_ChIP_S-50-H	ChIP	AY2	Single-end (50 bp)	19286579	79	97.72%	SRR2559331
RAD52-FLAG	AYY182	4h + gal	15-06-10_1st_ay_w303_Rad52flag_WT_4h_input_S-50-H	Input	AY3	Single-end (50 bp)	23173512	94	97.33%	SRR2559343
RAD52-FLAG	AYY182	4h + gal	15-06-10_1st_ay_w303_Rad52flag_WT_4h_ChIP_S-50-H	ChIP	AY4	Single-end (50 bp)	19323387	79	97.65%	SRR2559344
MTEI-FLAG	AYY140	0h + gal	15-06-10_1st_ay_w303_YGR042wflag_WT_0h_input_S-50-H	Input	AY5	Single-end (50 bp)	18493194	91	97.58%	SRR2559345
MTEI-FLAG	AYY140	0h + gal	15-06-10_1st_ay_w303_YGR042wflag_WT_0h_ChIP_S-50-H	ChIP	AY6	Single-end (50 bp)	22666774	76	96.22%	SRR2559346
MTEI-FLAG	AYY140	4h + gal	15-06-10_1st_ay_w303_YGR042wflag_WT_4h_input_S-50-H	Input	AY7	Single-end (50 bp)	17839811	72	97.12%	SRR2559347
MTEI-FLAG	AYY140	4h + gal	15-06-10_1st_ay_w303_YGR042wflag_WT_4h_ChIP_S-50-H	ChIP	AY8	Single-end (50 bp)	15075923	62	97.50%	SRR2559348
MTEI-FLAG <i>mph1Δ</i>	AYY148	0h + gal	15-06-10_1st_ay_w303_YGR042wflag_mph1Δ_0h_input_S-50-H	Input	AY9	Single-end (50 bp)	25713709	105	97.27%	SRR2559349
MTEI-FLAG <i>mph1Δ</i>	AYY148	0h + gal	15-06-10_1st_ay_w303_YGR042wflag_mph1Δ_0h_ChIP_S-50-H	ChIP	AY10	Single-end (50 bp)	12812434	53	97.63%	SRR2559350
MTEI-FLAG <i>mph1Δ</i>	AYY148	4h + gal	15-06-10_1st_ay_w303_YGR042wflag_mph1Δ_4h_input_S-50-H	Input	AY11	Single-end (50 bp)	14973419	61	97.03%	SRR2559333
MTEI-FLAG <i>mph1Δ</i>	AYY148	4h + gal	15-06-10_1st_ay_w303_YGR042wflag_mph1Δ_4h_ChIP_S-50-H	ChIP	AY12	Single-end (50 bp)	12793985	52	97.46%	SRR2559334
MPHI-FLAG <i>mte1Δ</i>	AYY155	0h + gal	15-06-10_1st_ay_w303_Mph1flag_ygr042wΔ_0h_input_S-50-H	Input	AY13	Single-end (50 bp)	17581434	71	96.82%	SRR2559335
MPHI-FLAG <i>mte1Δ</i>	AYY155	0h + gal	15-06-10_1st_ay_w303_Mph1flag_ygr042wΔ_0h_ChIP_S-50-H	ChIP	AY14	Single-end (50 bp)	14024187	57	97.36%	SRR2559336
MPHI-FLAG <i>mte1Δ</i>	AYY155	4h + gal	15-06-10_1st_ay_w303_Mph1flag_ygr042wΔ_4h_input_S-50-H	Input	AY15	Single-end (50 bp)	13983994	57	97.25%	SRR2559337
MPHI-FLAG <i>mte1Δ</i>	AYY155	4h + gal	15-06-10_1st_ay_w303_Mph1flag_ygr042wΔ_4h_ChIP_S-50-H	ChIP	AY16	Single-end (50 bp)	12879861	52	97.13%	SRR2559338
MPHI-FLAG	AYY156	0h + gal	15-06-10_1st_ay_w303_Mph1flag_WT_0h_input_S-50-H	Input	AY17	Single-end (50 bp)	17363022	71	97.34%	SRR2559339
MPHI-FLAG	AYY156	0h + gal	15-06-10_1st_ay_w303_Mph1flag_WT_0h_ChIP_S-50-H	ChIP	AY18	Single-end (50 bp)	13779730	56	96.81%	SRR2559340
MPHI-FLAG	AYY156	4h + gal	15-06-10_1st_ay_w303_Mph1flag_WT_4h_input_S-50-H	Input	AY19	Single-end (50 bp)	15831080	64	97.04%	SRR2559341
MPHI-FLAG	AYY156	4h + gal	15-06-10_1st_ay_w303_Mph1flag_WT_4h_ChIP_S-50-H	ChIP	AY20	Single-end (50 bp)	12284973	50	97.57%	SRR2559342

Table S3. GFP fusion proteins that co-localize with Rad52 during phleomycin treatment (percent of foci)

GFP-protein	ORF	% of GFP-Xxx foci that overlap Rad52 foci	% of Rad52 foci that overlap GFP-Xxx foci	# of Rad52-RFP foci	# of Xxx-GFP foci	Number of cells	Previously described co-localization with Rad52
Srs2	YJL092W	78.9	29.4	51	19	201	yes ^a
Rad59	YDL059C	54.5	30.0	20	11	147	yes ^b
Ygr042w	YGR042W	54.4	46.8	158	136	889	
Rad57	YDR004W	53.3	9.8	82	15	216	
Rad55	YDR076W	52.6	23.3	43	19	315	
Ddc2	YDR499W	47.1	71.4	91	138	197	yes ^b
Mgs1	YNL218W	43.2	35.6	90	74	482	
Dna2	YHR164C	40.7	61.2	139	209	641	yes ^b
Top3	YLR234W	37.5	12.5	24	8	185	
Rad53	YPL153C	34.8	25.0	96	69	329	
Rfa1	YAR007C	34.5	78.4	37	84	103	yes ^c
Rad9	YDR217C	34.0	39.5	43	50	227	yes ^b
Dpb11	YJL090C	31.3	57.7	26	48	102	yes ^d
Rmi1	YPL024W	30.4	12.1	58	23	318	
Rad54	YGL163C	30.2	30.2	43	43	166	yes ^b
Rfa2	YNL312W	27.4	65.4	26	62	59	yes ^b
Sgs1	YMR190C	26.3	12.5	40	19	162	
Ddc1	YPL194W	24.3	71.4	35	103	118	yes ^b
Rtt107	YHR154W	18.8	26.1	23	32	131	
Rad24	YER173W	17.6	2.0	153	17	430	
Rdh54	YBR073W	16.3	31.3	67	129	402	
Slx4	YLR135W	14.0	30.8	26	57	169	
Rtt101	YJL047C	12.5	4.5	111	40	563	
Mms21	YEL091C	9.3	8.0	50	43	258	
Mre11	YMR224C	9.1	7.7	39	33	123	yes ^b
Slx8	YER116C	8.0	3.1	64	25	281	
Rad5	YLR032W	7.0	5.0	80	57	676	
Rad50	YNL250W	4.0	3.6	55	50	244	
Csm1	YCR086W	1.7	1.6	63	60	269	

^a Burgess, R.C., Lisby M., Altmannova V., Krejci L., Sung P., and Rothstein R, 2009 Localization of recombination proteins and Srs2 reveals anti-recombinase function in vivo. *The Journal of Cell Biology* 185(6):969-981

^b Lisby, M., J.H. Barlow, R.C. Burgess, and R. Rothstein, 2004 Choreography of the DNA Damage Response; Spatiotemporal Relationships among Checkpoint and Repair Proteins. *Cell* 118 (6):699-713

^c Zhu, Z., Chung, W.H., Shim, E.Y., Lee, S.E., Ira, G, 2008 Sgs1 helicase and two nucleases Dna2 and Exo1 resect DNA double-strand break ends. *Cell* 134(6): 981-994

^d Germann, S.M., Oestergaard, V.H., Haas, C., Salis, P., Motegi, A., and Lisby, M, 2011 Dpb11/TopBP1 plays distinct roles in DNA replication, checkpoint response and homologous recombination. *DNA Repair (Amst)* 10(2):210-224

Pink shading indicates Xxx-GFP co-localizations less frequent than Mre11-GFP, and so should be regarded with caution.

Table S4. GFP fusion proteins that co-localize with Rad52 during phleomycin treatment (percent of cells)

GFP-protein	ORF	Number of cells	Percent of cells with Rad52-RFP foci	Percent of cells with Xxx-GFP foci	Percent of cells with co-localized foci
Ddc1	YPL194W	197	8.6	24.9	27.4
Rfa1	YAR007C	103	7.8	36.9	24.3
Rfa2	YNL312W	59	13.6	39.0	22.0
Ddc2	YDR499W	118	5.9	39.0	19.5
Dpb11	YJL090C	102	5.9	28.4	13.7
Dna2	YHR164C	641	5.0	14.2	12.5
Ygr042w	YGR042W	889	9.0	6.0	7.5
Rad9	YDR217C	227	11.0	13.2	7.5
Srs2	YJL092W	201	16.4	2.0	7.5
Rad53	YPL153C	329	17.9	14.9	6.7
Rad54	YGL163C	166	16.9	14.5	6.6
Mgs1	YNL218W	482	10.6	7.3	5.8
Rdh54	YBR073W	402	10.2	23.4	5.0
Rtt107	YHR154W	131	13.0	16.0	4.6
Slx4	YLR135W	169	10.7	23.1	4.1
Rad59	YDL059C	147	7.5	3.4	4.1
Rad57	YDR004W	216	27.8	2.8	3.7
Rad55	YDR076W	315	9.8	2.9	3.2
Top3	YLR234W	162	19.8	8.6	3.1
Mre11	YMR224C	123	23.6	21.1	2.4
Rmi1	YPL024W	318	14.2	4.1	2.2
Sgs1	YMR190C	185	10.8	2.7	1.6
Mms21	YEL091C	258	17.4	15.1	1.6
Rtt101	YJL047C	563	18.7	6.0	0.9
Rad50	YNL250W	244	19.3	16.4	0.8
Slx8	YER116C	281	19.9	7.1	0.7
Rad5	YLR032W	676	10.1	7.0	0.6
Rad24	YER173W	430	28.4	3.3	0.5
Csm1	YCR086W	269	21.9	23.8	0.4

Table S5. GFP fusion proteins that do not co-localize with Rad52 during phleomycin treatment (percent of cells)

GFP-protein	ORF	Number of cells	Percent of cells with Rad52-RFP foci	Percent of cells with Xxx-GFP foci	Number of Xxx-GFP foci	Percent of cells with co-localized foci
Oaf3	YKR064W	179	31.8	48.0	104	0
Yku70	YMR284W	335	18.2	24.5	100	0
Atg29	YPL166W	152	44.1	46.7	82	0
Crm1	YGR218W	206	19.9	25.7	78	0
Tub1	YML085C	235	20.4	17.0	37	0
Rrb1	YMR131C	255	15.3	12.2	32	0
Cdc27	YBL084C	189	8.7	7.2	31	0
Ymr111c	YMR111C	116	25.0	23.3	31	0
Pso2	YMR137C	356	23.3	7.9	30	0
Mrt4	YKL009W	132	23.5	17.4	23	0
Cgr1	YGL029W	164	21.3	10.4	17	0
Lsb1	YGR136W	227	30.8	5.3	15	0
Mrc1	YCL061C	261	25.7	5.4	15	0
Pph21	YDL134C	228	28.1	4.4	14	0
Tof2	YKR010C	109	11.9	11.9	14	0
Xrs2	YDR369C	280	10.7	5.0	14	0
Dus3	YLR401C	248	29.0	4.0	11	0
Pph3	YDR075W	201	20.4	5.0	9	0
Hta2	YBL003C	325	11.7	2.8	9	0
Edc2	YER035W	250	24.0	4.0	8	0
Ylr363w-a	YLR363W-A	180	27.8	4.4	8	0
Hos2	YGL194C	207	28.0	3.4	7	0
Apj1	YNL077W	186	24.2	3.2	6	0
Csm3	YMR048W	138	52.2	3.6	6	0
Rfc2	YJR068W	224	23.7	2.2	5	0
Ylr126c	YLR126C	193	23.8	4.1	5	0
Dug2	YBR281C	104	19.2	3.8	4	0
Rfc3	YNL290W	198	18.2	1.5	4	0
Rps18A	YDR450W	216	14.4	0.9	2	0
Pph22	YDL188C	248	21.8	0.8	2	0
Rfc5	YBR087W	199	39.7	0.5	1	0
Cmr1	YDL156W	198	25.3	0.0	0	0 ^a

^a No Xxx-GFP foci were detected.

Table S6. Genes that affect MteI-GFP focus formation

Standard Name	Systematic Name	Result ^a		Detected in quantitative analysis ^b
		Control	2 hours + phleo	
<i>MGS1</i>	<i>YNL218W</i>	unchanged	decreased	no
<i>MPH1</i>	<i>YIL002</i>	unchanged	decreased	yes
<i>RFA2-ph</i>	<i>YNL312W</i>	unchanged	decreased	yes
<i>RAD24</i>	<i>YER173W</i>	unchanged	increased	no
<i>RAD59</i>	<i>YDL059C</i>	unchanged	increased	no
<i>SLX8</i>	<i>YER116C</i>	unchanged	increased	no
<i>TOP3</i>	<i>YLR234W</i>	unchanged	increased	no
<i>MRE11</i>	<i>YMR224C</i>	unchanged	unchanged	yes
<i>RAD9</i>	<i>YDR217C</i>	unchanged	increased	yes
<i>RAD50</i>	<i>YGR017W</i>	increased	increased	yes
<i>RAD52</i>	<i>YML032C</i>	increased	increased	yes
<i>XRS2</i>	<i>YDR369C</i>	increased	increased	yes
<i>APJ1</i>	<i>YNL077W</i>	unchanged	unchanged	
<i>ATG29</i>	<i>YPL166W</i>	unchanged	unchanged	
<i>CMR1</i>	<i>YDL156W</i>	unchanged	unchanged	
<i>CSM1</i>	<i>YCR086W</i>	unchanged	unchanged	
<i>CSM3</i>	<i>YMR048W</i>	unchanged	unchanged	
<i>DDC1</i>	<i>YPL194W</i>	unchanged	unchanged	
<i>DUG1</i>	<i>YBR281C</i>	unchanged	unchanged	
<i>DUS3</i>	<i>YLR401C</i>	unchanged	unchanged	
<i>EDC2</i>	<i>YER035W</i>	unchanged	unchanged	
<i>HOS2</i>	<i>YGL194C</i>	unchanged	unchanged	
<i>HPR5/SRS2</i>	<i>YJL092W</i>	unchanged	unchanged	
<i>HTA2</i>	<i>YBL003C</i>	unchanged	unchanged	
<i>LSB1</i>	<i>YGR136W</i>	unchanged	unchanged	
<i>MMS2</i>	<i>YGL087C</i>	unchanged	unchanged	
<i>MMS4</i>	<i>YBR098W</i>	unchanged	unchanged	
<i>MRC1</i>	<i>YCL061C</i>	unchanged	unchanged	
<i>MRT4</i>	<i>YKL009W</i>	unchanged	unchanged	
<i>OAF3</i>	<i>YKR064W</i>	unchanged	unchanged	
<i>PPH21</i>	<i>YDL134C</i>	unchanged	unchanged	
<i>PPH22</i>	<i>YDL188C</i>	unchanged	unchanged	
<i>PPH3</i>	<i>YDR075W</i>	unchanged	unchanged	
<i>PSO2</i>	<i>YMR137C</i>	unchanged	unchanged	
<i>RAD5</i>	<i>YLR032W</i>	unchanged	unchanged	
<i>RAD54</i>	<i>YGL163C</i>	unchanged	unchanged	
<i>RAD55</i>	<i>YDR076W</i>	unchanged	unchanged	
<i>RAD57</i>	<i>YDR004W</i>	unchanged	unchanged	
<i>RFA3-313</i>	<i>YJL173C</i>	unchanged	unchanged	
<i>RMII</i>	<i>YPL024W</i>	unchanged	unchanged	
<i>RPS18A</i>	<i>YDR450W</i>	unchanged	unchanged	
<i>RTT107</i>	<i>YHR154W</i>	unchanged	unchanged	
<i>SGS1</i>	<i>YMR190C</i>	unchanged	unchanged	
<i>SLX4</i>	<i>YLR135W</i>	unchanged	unchanged	
<i>TEL1</i>	<i>YBL088C</i>	unchanged	unchanged	
<i>TOF1</i>	<i>YNL273W</i>	unchanged	unchanged	
<i>TOF2</i>	<i>YKR010C</i>	unchanged	unchanged	
<i>UBC13</i>	<i>YDR092W</i>	unchanged	unchanged	
<i>YKU70</i>	<i>YMR284W</i>	unchanged	unchanged	
<i>YLR126C</i>	<i>YLR126C</i>	unchanged	unchanged	
<i>YLR363W-A</i>	<i>YLR363W-A</i>	unchanged	unchanged	
<i>YMR11C</i>	<i>YMR11C</i>	unchanged	unchanged	

^a MteI-GFP foci were detected by imaging a single z-slice in high throughput.

^b MteI-GFP foci were detected by imaging eleven z-slices by confocal fluorescence microscopy.